Vibronic Coupling Model for the Calculation of Mixed-Valence Line Shapes: The Interdependence of Vibronic and MO Effects

Susan B. Piepho

Contribution from the Department of Chemistry, Sweet Briar College, Sweet Briar, Virginia 24595. *Received December 21, 1987*

Abstract: A simplified vibronic coupling model is developed for mixed-valence systems. Like the PKS model, it provides explicit vibronic eigenvalues and eigenfunctions with which the absorption profile may be obtained for the full range of mixed-valence systems from the localized (class II) to the delocalized (class III). It differs from the PKS model in that *multi*-center vibrations (such as the A–B stretch in a simple A–B dimer) play an important role, while the PKS model includes vibronic coupling *only* to linear combinations of vibrations *localized on the metal ion centers*. We show that coupling to *both* types of vibrations is involved in even the simplest mixed-valence systems. A molecular orbital basis is used (as in the work of Ondrechen et al.) rather than the valence bond type basis of the PKS model. We show how vibronic coupling in mixed-valence compounds is similar to vibronic coupling in more "conventional" molecules and how Bersuker's orbital vibronic constants (OVC) may be used to parametrize this coupling. From this point of view, localized mixed-valence systems are those for which there is a strong pseudo-Jahn–Teller coupling in the $q_- = (1/\sqrt{2})(q_A - q_B)$ mode. We illustrate how the magnitude of the OVC may be estimated by consideration of the type of molecular orbitals and vibrations involved. This gives useful physical insight into which vibrations are apt to be strongly coupled vibronically in specific systems. A *simplified MO* model for mixed-valence dimers is first described, and results are presented for this model. It is shown that with the redefinition of the electronic interaction parameter Δ, these results may be used to explain the dominant features of typical mixed-valence systems.

I. Introduction

Inorganic mixed-valence compounds contain two or more metal ion centers in different oxidation states between which an electron can transfer. A well-known example is the Creutz–Taube ion,[1] μ-pyrazine-bis(pentaammineruthenium)$^{5+}$ (**1**). It contains two

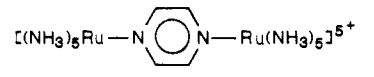

1

metal ion complexes ("monomers") connected by a bridging group. Such compounds serve as excellent models for the study of electron transfer, since the transfer takes place in a controlled, well-defined environment. Mixed-valence compounds are characterized by an intense relatively featureless absorption band in the near-infrared or visible which cannot be attributed to their "monomeric" components or bridging ligands. This "mixed-valence" band, which is associated with electron transfer, results from transitions within a ground vibronic manifold arising from the coupling of the constituent ions.

For the theoretician, even the simplest mixed-valence system is a challenge to characterize since electron transfer is a dynamic process; a change in nuclear configuration accompanies the electronic motion, and the coupling of electronic and vibrational motions is central to the problem. Early models of mixed-valence systems concentrated on the most fundamental aspects of the observed mixed-valence bands (their energy, width, and solvent dependence) and tried to explain these features with simplified models.[2,3] These models were quite successful in understanding the broad features of mixed-valence dimers in which the ions were very weakly coupled electronically. In such compounds there is some delocalization, but different distinct oxidation states are still identifiable on the two centers. Robin and Day[2] term these class II mixed-valence compounds.

These early models, however, are increasingly inapplicable as we move to systems in which both electronic and vibronic coupling are significant, that is as we pass from the more localized to the less localized class II systems or to delocalized class III mixed-valence compounds. Moreover they do not allow calculation of the mixed-valence absorption profile and are not designed to take into account the nature of metal ion states or bridging ligands in specific compounds.

Consideration of these limitations led us to formulate a vibronic coupling model for mixed-valence dimers with which to simulate the mixed-valence absorption band. This model, which is refered to as the PKS model,[4] is still a schematic one, but it represents a real improvement over earlier theoretical models[2,3] in that it is applicable to both class II and class III mixed-valence systems, and it allows explicit vibronic eigenvalues and eigenvectors to be determined. These are essential for meaningful calculation of various properties of mixed-valence compounds. Our initial paper used the PKS model to simulate mixed-valence band contours, and since that time the model has been used by a number of other researchers to analyze mixed-valence data. Much of this research is summarized in a review article by Wong and Schatz.[5] The model has also been extended to handle exchange-coupled mixed-valence dimers[6] and trinuclear mixed-valence compounds,[7-9] and to begin to explicitly include the bridge in the dimeric case.[10]

Ondrechen and co-workers[11] further advanced the understanding of mixed-valence systems by formulating a more realistic three-site model for delocalized (class III) bridged mixed-valence dimers which have the form A–B–C where A and C are metal

(1) Creutz, C.; Taube, H. *J. Am. Chem. Soc.* **1969**, *91*, 3988. Creutz, C.; Taube, H. *J. Am. Chem. Soc.* **1973**, *95*, 1086.
(2) Robin, M. B.; Day, P. *Adv. Inorg. Chem. Radiochem.* **1967**, *10*, 247.
(3) Hush, N. S. *Prog. Inorg. Chem.* **1967**, *8*, 391–444.
(4) Piepho, S. B.; Krausz, E. R.; Schatz, P. N. *J. Am. Chem. Soc.* **1978**, *100*, 2996–3005.
(5) Wong, K. Y.; Schatz, P. N. *Prog. Inorg. Chem.* **1981**, *28*, 369–449.
(6) Borshch, S. A.; Kotov, I. N.; Bersuker, I. B. *Chem. Phys. Lett.* **1984**, *111*, 264–270.
(7) Launay, J. P.; Babonneau, F. *Chem. Phys.* **1982**, *67*, 295–300.
(8) Borshch, S. A.; Kotov, I. N.; Bersuker, I. B. *Chem. Phys. Lett.* **1982**, *89*, 381–384.
(9) Cannon, R. D.; Montri, L.; Brown, D. B.; Marshall, K. M.; Elliott, C. M. *J. Am. Chem. Soc.* **1984**, *106*, 2591–2594.
(10) Neuenschwander, K.; Piepho, S. B.; Schatz, P. N. *J. Am. Chem. Soc.* **1985**, *107*, 7862–7869.
(11) (a) Root, L. J.; Ondrechen, M. J. *Chem. Phys. Lett.* **1982**, *93*, 421–424. (b) Ondrechen, M. J.; Ko, J.; Root, L. J. *J. Phys. Chem.* **1984**, *88*, 5919–5923. (c) Ko, J.; Ondrechen, M. J. *Chem. Phys. Lett.* **1984**, *112*, 507–512. (d) Ko, J.; Ondrechen, M. J. *J. Am. Chem. Soc.* **1985**, *107*, 6161–6167. (e) Ko, J.; Zhang, L.-T.; Ondrechen, M. J. *J. Am. Chem. Soc.* **1986**, *108*, 1712–1713. (f) Zhang, L.-T.; Ko, J.; Ondrechen, M. J. *J. Am. Chem. Soc.* **1987**, *109*, 1666–1671. (g) Ondrechen, M. J.; Ko, J.; Zhang, L.-T. *J. Am. Chem. Soc.* **1987**, *109*, 1672–1676.

0002-7863/88/1510-6319$01.50/0

ion centers and B is a bridging ligand. While this three-site model incorporates a number of features of the PKS model, it differs in that it explicitly includes the bridge and it uses a molecular orbital (multi-center) basis of one-electron functions. In contrast, the PKS model is a two-site model which uses a valence-bond type of electronic basis. In addition different vibrational modes figure prominantly in the Ondrechen and PKS models.

II. Current Objectives

The aim of the present paper is to formulate the simplest possible model that explains the dominant spectral features of mixed-valence systems and at the same time gives useful physical insight into the magnitude of vibronic and electronic coupling in specific systems. To this end we work consistently from a molecular orbital point of view. We show how vibronic coupling in mixed-valence compounds is similar to vibronic coupling in more "conventional" molecules and how Bersuker's[12] orbital vibronic constants (OVC) may be used to parametrize this coupling. The magnitude of these OVC can then often be estimated by consideration of the type of MO's and vibrations involved.

While the PKS model[4,5] includes vibronic coupling only to linear combinations of vibrations *localized on the metal centers* A and B, in this treatment *multi-center* vibrations (such as the A–B stretch in a simple A–B dimer) are shown to be important participants in the vibronic coupling. Thus even the simplest mixed-valence problems are two-mode problems. Whereas Ondrechen et al.[11] discuss only delocalized systems, our results are applicable to both localized (class II) and delocalized (class III) mixed-valence compounds. While we concentrate on very simple prototype mixed-valence systems, we argue in section VII that our results describe the dominant features of real mixed-valence systems.

III. *Simplified MO* Model for Mixed-Valence Dimers

We suppose our mixed-valence dimer A–B consists of two "monomeric" units, A and B. The dimer is assumed symmetrical so that A = B. The monomers are joined together via an unspecified bridge; in real mixed-valence complexes this bridge might be a single atom such as oxygen or a more complex molecule such as pyrazine.

Electronic Basis and Electronic Interactions. We begin with a highly simplified electronic basis which is largely symbolic since at this stage we ignore interactions with bridge orbitals. The important atomic orbitals in our *simplified MO* model are those that interact to form bonding/antibonding MO's. In our initial treatment we assume that the bonding MO (which we call γ) is fully occupied and that a single electron occupies the antibonding MO (designated γ^*). Thus our electronic basis states are

$$\varphi_1 = |\gamma^2\gamma^{*1}\rangle,\ \varphi_2 = |\gamma^1\gamma^{*2}\rangle \tag{1}$$

where the unpaired electron can have either $+^1/_2$ or $-^1/_2$ spin. The kets designate Slater determinants. These states differ in energy by Δ, where the magnitude of Δ is expected to be large when the bonding/antibonding interaction is significant. Thus Δ is a measure of the electronic interaction between the atomic orbitals centered on A and B which results in the formation of the γ and γ^* MO's; it is analogous to ϵ in the PKS model.[4]

We emphasize that this basis is not particularly realistic. However, we show in section VII that while explicit consideration of the bridge necessitates use of a more complete basis, this *simplified MO* basis is sufficient to describe the principal features of mixed-valence systems.

Vibrational Basis and Vibronic Interactions. Strong vibronic interactions involve vibrational coordinates that change significantly during adiabatic electron transfer. In the localized picture, stable states of our A–B complex would be those with A oxidized and B reduced or vice versa: $A^{ox}B^{red}$ and $A^{red}B^{ox}$. A totally symmetric coordinate of A (Q_A) changes the shorter equilibrium bond lengths of the oxidized form to those of the reduced form, and likewise for B; thus the symmetry-adapted linear combinations of these single-center (localized = loc) coordinates are part of our vibrational basis:

$$Q_+^{loc} = (1/\sqrt{2})(Q_A + Q_B) \tag{2}$$

$$Q_-^{loc} = (1/\sqrt{2})(Q_A - Q_B) \tag{3}$$

These modes, and only these modes, were included in the PKS model;[4,5] it was then shown that Q_+^{loc} made no contribution, so the PKS model reduced to a one-mode (Q_-^{loc}) problem.

In the delocalized picture, stable states of our A–B complex are those of eq 1. The coordinate that connects the longer A–B equilibrium bond lengths of the antibonding excited state φ_2 with those of the ground state φ_1 is the totally symmetric (molecular = mol) A–B stretching coordinate $Q_+^{mol} = Q_{AB}$. This mode has no single-center analogue; it is an additional totally symmetric mode that arises when A and B come together to form A–B. Q_{AB} is expected to play an important role in determining the bandshape in the delocalized case since in that limit the bonding/antibonding interaction is large. Conversely, Q_-^{loc} plays the major role in more localized mixed-valence systems.

In real mixed-valence compounds a bridge connects A and B. Thus the antibonding/bonding interactions and the A–B stretching mode would involve the bridge orbitals and bridge stretching motions. The types of interactions, however, remain the same.

IV. The Vibronic Matrix

We write our total molecular Hamiltonian as

$$H_T(q,Q) = H_{el}(q,Q) + T_N(Q) \tag{4}$$

where

$$H_{el}(q,Q) = T_e(q) + V_{ee}(q) + V(q,Q) \tag{5}$$

The q,Q represent electronic and nuclear coordinates, respectively. T_N and T_e are the nuclear and electronic kinetic energy operators, V_{ee} is the operator for interelectronic electrostatic interactions, and $V(q,Q)$ is the operator for electron–nuclear (vibronic) interactions plus internuclear repulsions. Our zero-order electronic functions $\varphi_j^0 \equiv \varphi_j(q,Q_0)$ are solutions to $H_{el}(q,Q)$ at the ground-state nuclear configuration $Q_0 = 0$:

$$H_{el}(q,Q_0)\varphi_j^0 = W_j^0(Q_0)\varphi_j^0 \tag{6}$$

In order to see the effect of nuclear displacements on the φ_j^0, the Schrödinger equation for the total (dynamic) Hamiltonian must be solved. We begin by rewriting $H_T(q,Q)$ of eq 4 to give

$$H_T(q,Q)\Psi_r(q,Q) = (H_{el}(q,Q_0) + T_N(Q) + W(q,Q))\Psi_r(q,Q) = E_r\Psi_r(q,Q) \tag{7}$$

where

$$\Psi_r(q,Q) = \sum_j \varphi_j^0 \chi_{jr}(Q) \tag{8}$$

$$W(q,Q) = V(q,Q) - V(q,Q_0) \tag{9}$$

Here the electronic basis states φ_j^0 are assumed to be unperturbed by vibronic interaction with electronic states *outside* the basis. Since they are independent of Q, they commute with T_N; they may, however, be mixed with one another by $W(q,Q)$. Central to our treatment (and to the older PKS model[4,5]) is the fact that *we do not make the Born–Oppenheimer approximation*, and the electronic basis states are coupled vibronically; thus nuclear motion is *not confined to a single surface*. The φ_j^0 may be mixed significantly by vibronic interactions. The model may thus be applied to the full range of mixed-valence systems from the localized (class II) to the delocalized (class III) using the same electronic basis in each case.

Solving eq 7 reduces to solving the set of coupled equations

$$\sum_{j'=1}^{n} [(T_N + W_j^0 - E_r)\delta_{jj'} + W_{jj'}(Q)]\chi_{j'r}(Q) = 0\ (j = 1, \ldots, n) \tag{10}$$

where

(12) Bersuker, I. B. *The Jahn-Teller Effect and Vibronic Interactions in Modern Chemistry*; Plenum: New York, 1984.

$$W_{jj'}(Q) = \langle \varphi_j^0 | W(q,Q) | \varphi_{j'}^0 \rangle \quad (11)$$

When $W_{jj'}(Q) \neq 0$, the potential surfaces associated with the electronic basis states are vibronically coupled, and the Born–Oppenheimer approximation breaks down. We make the harmonic approximation and solve eq 10 using a harmonic oscillator basis; see eq 24 and 28 ahead. But when $W_{jj'}(Q) \neq 0$, the $\chi_{jr}(Q)$ are *not* in general simple products of harmonic oscillator functions.

Making the harmonic approximation and using normal coordinates, the operator for vibronic interactions $W(q,Q)$ may be expressed as

$$W(q,Q) \approx \sum_\alpha (\partial V/\partial Q_\alpha)_{Q_0} Q_\alpha + (1/2)\sum_{\alpha,\beta}[(\partial^2 V/\partial Q_\alpha \partial Q_\beta)_{Q_0}] Q_\alpha Q_\beta \quad (12)$$

We neglect higher order terms. If the ground-state nuclear coordinates are chosen so that $Q_0 = 0$ at the potential minima, then $(\partial V/\partial Q_\alpha)_{Q_0} = 0$ for all α of the ground state. Likewise the Q may be chosen for the ground state so that the cross-terms $Q_\alpha Q_\beta$ in $W(q,Q)$ vanish; for other states we neglect these cross terms.

We then define

$$l_\alpha^{(j)} = \langle \varphi_j^0 | (\partial V/\partial Q_\alpha)_{Q_0} | \varphi_j^0 \rangle \quad (13)$$

$$l_\alpha^{(jj')} = \langle \varphi_j^0 | (\partial V/\partial Q_\alpha)_{Q_0} | \varphi_{j'}^0 \rangle \quad (14)$$

$$k_\alpha^{(j)} = \langle \varphi_j^0 | (\partial^2 V/\partial Q_\alpha^2)_{Q_0} | \varphi_j^0 \rangle \quad (15)$$

where the l's are linear vibronic constants and the k's are force constants. With these definitions and approximations, we have

$$W_{jj}(Q) = \sum_\alpha (l_\alpha^{(j)} Q_\alpha + (1/2) k_\alpha^{(j)} Q_\alpha^2) \quad (16)$$

$$W_{jj'}(Q) = \sum_\alpha l_\alpha^{(jj')} Q_\alpha \quad (17)$$

where, as discussed above, for the ground state the $l_\alpha^{(j)} = l_\alpha^{(1)} = 0$. Finally we transform to dimensionless variables

$$q_\alpha = \hbar^{-1}(h\upsilon_\alpha)^{1/2} Q_\alpha \quad (18)$$

$$\lambda_\alpha^{(j)} = \hbar (h\upsilon_\alpha)^{-1/2} (\sqrt{2} h\upsilon_\alpha)^{-1} l_\alpha^{(j)} \quad (19)$$

where $\upsilon_\alpha = (1/2\pi)\sqrt{k_\alpha}$ is the fundamental vibrational frequency associated with normal coordinate Q_α. Thus

$$W_{jj}(q) = \sqrt{2}\sum_\alpha h\upsilon_\alpha [\lambda_\alpha^{(j)} q_\alpha + (1/2) q_\alpha^2]$$

$$W_{jj'}(q) = \sqrt{2}\sum_\alpha h\upsilon_\alpha \lambda_\alpha^{(jj')} q_\alpha \quad (20)$$

V. Vibronic Matrix for the *Simplified MO* Model

We assume our mixed-valence complex has D_{2h} symmetry. Our active vibrational coordinates transformed to dimensionless variables are thus

$$q_1 = q_{A_{1g}}^{mol} = q_{AB}$$

$$q_2 = q_- = q_{B_{1u}}^{loc} = (1/\sqrt{2})(q_A - q_B)$$

$$q_3 = q_{A_{1g}}^{loc} = (1/\sqrt{2})(q_A + q_B) \quad (21)$$

The electronic ground and excited states of eq 1 become

$$\varphi_1^{\pm} = \varphi^{\pm}(^2B_{2g}) = |b_{3u}^2 b_{2g}^{\pm}\rangle$$
$$\varphi_2^{\pm} = \varphi^{\pm}(^2B_{3u}) = |b_{3u}^{\pm} b_{2g}^2\rangle \quad (22)$$

assuming $\gamma = b_{3u}$ and $\gamma^* = b_{2g}$. These symmetries are typical of an A–B type mixed-valence complex with A = B and with a π-type interaction between d orbitals on the two centers and the bridge. Symmetry considerations and our discussions above then give the electronic potential energy matrix

$$\begin{bmatrix} 0 & h\upsilon_2\sqrt{2}\lambda_2^{(1,2)} q_2 \\ h\upsilon_2\sqrt{2}\lambda_2^{(1,2)} q_2 & \Delta + \sqrt{2}[h\upsilon_1\lambda_1^{(2)} q_1 + h\upsilon_3\lambda_3^{(2)} q_3] \end{bmatrix} \quad (23)$$

Nuclear kinetic energy terms are then added to the above and this *dynamic* matrix is diagonalized in the

$$\Phi_s \equiv [\Phi_{jn_1n_2n_3}]_s \equiv [\varphi_j^0 \chi_1^{n_1} \chi_2^{n_2} \chi_3^{n_3}]_s \quad (24)$$

basis where the φ_j^0 are those of eq 22 and the χ's are harmonic oscillator functions in the respective coordinates q_1, q_2, and q_3. Diagonal matrix elements are

$$\langle \Phi_{1n_1n_2n_3} | H_T | \Phi_{1n_1n_2n_3} \rangle = \sum_{i=1}^{3} (n_i + 1/2) h\upsilon_i$$

$$\langle \Phi_{2n_1n_2n_3} | H_T | \Phi_{2n_1n_2n_3} \rangle = \Delta + \sum_{i=1}^{3} (n_i + 1/2) h\upsilon_i \quad (25)$$

and non-zero off-diagonal elements are

$$\langle \Phi_{2n_1n_2n_3} | H_T | \Phi_{2n_1'n_2n_3} \rangle = \left\{ \left(\frac{n_1 + 1}{2} \right)^{1/2} \delta_{n_1', n_1+1} + \left(\frac{n_1' + 1}{2} \right)^{1/2} \delta_{n_1, n_1'+1} \right\} \sqrt{2} h\upsilon_1 \lambda_1^{(2)}$$

$$\langle \Phi_{2n_1n_2n_3} | H_T | \Phi_{2n_1n_2n_3'} \rangle = \left\{ \left(\frac{n_3 + 1}{2} \right)^{1/2} \delta_{n_3', n_3+1} + \left(\frac{n_3' + 1}{2} \right)^{1/2} \delta_{n_3, n_3'+1} \right\} \sqrt{2} h\upsilon_3 \lambda_3^{(2)}$$

$$\langle \Phi_{2n_1n_2n_3} | H_T | \Phi_{1n_1n_2'n_3} \rangle = \langle \Phi_{1n_1n_2n_3} | H_T | \Phi_{2n_1n_2'n_3} \rangle = \left\{ \left(\frac{n_2 + 1}{2} \right)^{1/2} \delta_{n_2', n_2+1} + \left(\frac{n_2' + 1}{2} \right)^{1/2} \delta_{n_2, n_2'+1} \right\} \sqrt{2} h\upsilon_2 \lambda_2^{(1,2)} \quad (26)$$

This basis is, in principle, infinite in each of n_1, n_2, and n_3. However, we truncate the basis by limiting the *total number* of excited vibrational quanta to n. Thus,

$$n_1 = 0, 1, \ldots, n$$

$$n_2 = 0, 1, \ldots, n$$

$$n_3 = 0, 1, \ldots, n$$

with

$$(n_1 + n_2 + n_3) \leq n \quad (27)$$

Diagonalization of the dynamic matrix gives eigenvalues and eigenfunctions for the dynamic problem. These may be determined to arbitrary accuracy by choosing n sufficiently large. They may then be used to calculate observables for the system. Eigenfunctions have the form

$$\Psi_r(q,Q) = \sum_j \varphi_j^0 \chi_{jr}(Q) = \sum_s c_{rs} [\varphi_{jn_1n_2n_3}]_s = \sum_s c_{rs} \Phi_s \quad (28)$$

where the sum over s includes all the n_s allowed combinations of j, n_1, n_2, and n_3. The notation for Φ_s is that of eq 24. If n is the maximum number of vibrational quanta (see eq 27) and m is the number of electronic states (here $m = 2$) then the dimension of our matrix n_s for the three-mode problem described above is

$$n_s(\text{three-mode}) = (m)(n + 1)(n + 2)(n + 3)/6 \quad (29)$$

If one of the modes decouples, the resulting two-mode problem has a dimension of

$$n_s(\text{two-mode}) = (m)(n + 1)(n + 2)/2 \quad (30)$$

To obtain the profile of the mixed-valence band, we calculate the dipole strength of each vibronic line. The $\varphi_1 \rightarrow \varphi_2$ electronic transition is z polarized. For the transition $\Psi_r(q,Q) \rightarrow \Psi_{r'}(q,Q)$

$$D(r \rightarrow r') = [(N_r - N_{r'})/N] \, |\langle \Psi_r | m_z | \Psi_{r'} \rangle|^2 \quad (31)$$

where

$$N_r = \exp(-E_r/kT),\ N = \sum_r N_r \tag{32}$$

and

$$\langle \Psi_r|m_z|\Psi_{r'}\rangle = \sum_{s=1}^{n_s}\sum_{s'=1}^{n_s} c_{rs}c_{r's'}\langle \Phi_s|m_z|\Phi_{s'}\rangle$$

$$= \sum_{s=1}^{n_s}\sum_{s'=1}^{n_s} c_{rs}c_{r's'}\langle [\varphi_{jn_1n_2n_3}]_s|m_z|[\varphi_{j'n_1'n_2'n_3'}]_{s'}\rangle$$

$$= \sum_{s=1}^{n_s}\sum_{s'=1}^{n_s} c_{rs}c_{r's'}[(\delta_{j,j'+1} + \delta_{j+1,j'})\delta_{n_1n_1'}\delta_{n_2n_2'}\delta_{n_3n_3'}]_{s,s'}\langle \varphi_1{}^0|m_z|\varphi_2{}^0\rangle$$

$$\equiv S_{ss'}\langle \varphi_1{}^0|m_z|\varphi_2{}^0\rangle \tag{33}$$

Magnitude of Vibronic Constants. Bersuker[12] has shown how the linear vibronic constants, the l of eq 13 and 14 and hence the λ of eq 19, may be expressed in terms of orbital vibronic constants (OVC's) and how the magnitudes of the diagonal OVC's may be estimated. The OVC's have the form $\langle\gamma|(\partial v(i)/\partial Q_\alpha)_{Q_0}|\gamma'\rangle$ where γ and γ' are molecular orbitals. We apply his method below.

Since $(\partial V/\partial Q_\alpha)_{Q_0}$ is a one-electron operator, we can write

$$\left(\frac{\partial V}{\partial Q_\alpha}\right)_{Q_0} = \sum_{i=1}^{3}\left(\frac{\partial v(i)}{\partial Q_\alpha}\right)_{Q_0} \tag{34}$$

and thus for $\alpha = 1, 3$

$$\begin{aligned} l_\alpha^{(1)} &= \left\langle \varphi_1{}^0\middle|\left(\frac{\partial V}{\partial Q_\alpha}\right)_{Q_0}\middle|\varphi_1{}^0\right\rangle \\ &= \left\langle b_{3u}{}^2b_{2g}{}^{\pm}\middle|\left(\frac{\partial V}{\partial Q_\alpha}\right)_{Q_0}\middle|b_{3u}{}^2b_{2g}{}^{\pm}\right\rangle \\ &= 2\left\langle b_{3u}\middle|\left(\frac{\partial v(i)}{\partial Q_\alpha}\right)_{Q_0}\middle|b_{3u}\right\rangle + \left\langle b_{2g}\middle|\left(\frac{\partial v(i)}{\partial Q_\alpha}\right)_{Q_0}\middle|b_{2g}\right\rangle \\ &= 0 \end{aligned} \tag{35}$$

The last equality follows from our choice of nuclear coordinates: we have $Q_0 = 0$ at the ground-state potential minimum for all α. Also for $\alpha = 1, 3$

$$\begin{aligned} l_\alpha^{(2)} &= \left\langle \varphi_2{}^0\middle|\left(\frac{\partial V}{\partial Q_\alpha}\right)_{Q_0}\middle|\varphi_2{}^0\right\rangle \\ &= \left\langle b_{3u}\middle|\left(\frac{\partial v(i)}{\partial Q_\alpha}\right)_{Q_0}\middle|b_{3u}\right\rangle + 2\left\langle b_{2g}\middle|\left(\frac{\partial v(i)}{\partial Q_\alpha}\right)_{Q_0}\middle|b_{2g}\right\rangle \\ &= -\left\langle b_{3u}\middle|\left(\frac{\partial v(i)}{\partial Q_\alpha}\right)_{Q_0}\middle|b_{3u}\right\rangle + \left\langle b_{2g}\middle|\left(\frac{\partial v(i)}{\partial Q_\alpha}\right)_{Q_0}\middle|b_{2g}\right\rangle \end{aligned} \tag{36}$$

where in the last equality we have subtracted out the zero sum from eq 35. Finally,

$$\begin{aligned} l_2^{(1,2)} = l_2^{(2,1)} &= \left\langle \varphi_2{}^0\middle|\left(\frac{\partial V}{\partial Q_2}\right)_{Q_0}\middle|\varphi_1{}^0\right\rangle \\ &= -\left\langle b_{2g}\middle|\left(\frac{\partial v(i)}{\partial Q_2}\right)_{Q_0}\middle|b_{3u}\right\rangle \end{aligned} \tag{37}$$

Bersuker then goes on to give a very useful interpretation to each *diagonal* OVC for the ith MO and a totally symmetric vibrational mode v_α: it is equal to the *force with which an electron in the MO distorts the nuclear framework in the direction of the totally symmetric displacement* Q_α minus the proportion of the internuclear repulsion in this direction per electron.[12] This means for a vibrational coordinate such as $Q_1 = Q_{AB}$ which affects the internuclear A–B bond length, diagonal OVC are most often *positive* for MO's *bonding* with respect to the A–B bond, *negative* for MO's *antibonding*, and ca. zero for MO's *nonbonding* with respect to the A–B bond. The OVC magnitude for a given totally symmetric vibration Q_α is related to the sensitivity of the MO to motion along the coordinate Q_α. Thus vibronic and molecular orbital effects are interdependent.

Application to Simplified MO Model. Applying Bersuker's interpretation of the diagonal OVC to our problem, we see that the OVC in $Q_1 = Q_{A_{1g}}{}^{mol} = Q_{AB}$ should be *negative* for the antibonding b_{2g} MO and *positive* for the bonding b_{3u} MO. Thus the terms in eq 36 for $l_1^{(2)}$ should be *additive* to give a negative result. Moreover, if the bonding/antibonding interaction is large as in delocalized mixed-valence complexes, $l_1^{(2)}$ should likewise be large.

On the other hand $l_3^{(2)}$, the diagonal OVC for $Q_3 = Q_{A_{1g}}{}^{loc} = (1/\sqrt{2})(Q_A + Q_B)$, should be zero for our *simplified MO* mixed-valence model. This follows since from eq 2 or 21 we have

$$\left(\frac{\partial V}{\partial Q_3}\right)_{Q_{2,..}} = \frac{1}{\sqrt{2}}\left[\left(\frac{\partial V}{\partial Q_A}\right)_{Q_{B,..}} + \left(\frac{\partial V}{\partial Q_B}\right)_{Q_{A,..}}\right] \tag{38}$$

and from the discussion accompanying eq 1 and 22 it follows that our MO's have the form

$$\begin{aligned} |b_{2g}\rangle &= \frac{1}{\sqrt{2}}(|b_2(A)\rangle + |b_2(B)\rangle) \\ |b_{3u}\rangle &= \frac{1}{\sqrt{2}}(|b_2(A)\rangle - |b_2(B)\rangle) \end{aligned} \tag{39}$$

where $|b_2(A)\rangle$ and $|b_2(B)\rangle$ could be d orbitals centered on A and B respectively which interact to form the bonding b_{3u} and antibonding b_{2g} MO's. We assume the A and B units which comprise our A–B mixed-valence complex have C_{2v} local symmetry; b_2 is a C_{2v} symmetry label. Substituting eq 38 and 39 into eq 36 for $Q_\alpha = Q_3$ gives $l_3^{(2)} = 0$ and thus $\lambda_3^{(2)} = 0$.

There is no such simple physical interpretation for the off-diagonal OVC's. They govern the magnitude of the pseudo-Jahn–Teller (PJT) effect. In our *simplified MO* mixed-valence model the PJT-active mode is $Q_2 = Q_{B_{1u}}{}^{loc} = (1/\sqrt{2})(Q_A - Q_B)$, the Q_- mode of the PKS model.[4] It induces vibronic coupling between our basis states via the OVC of eq 37. When the PJT effect for this mode is large (i.e., $l_2^{(1,2)}$, and hence $\lambda_2^{(1,2)}$, is large), the mixed-valence compound is *localized*. This will be illustrated ahead where we plot the probability distribution $P(q_2)$ in $q_2 = q_-$ space versus q_2. When $\lambda_2^{(1,2)}$ is large, the probability peaks away from $q_- = 0$ and we have a *localized* mixed-valence complex. $\lambda_2^{(1,2)}$ is directly analogous to λ^{PKS}, the λ parameter of the PKS model.[4]

The PKS model predicts λ^{PKS} will be proportional to the difference in bond lengths between the oxidized and reduced forms of the monomer. The same should be true here for $\lambda_2^{(1,2)}$ since we now show $\lambda_2^{(1,2)}$ reduces to essentially the same OVC. Analogous to eq 38 we have

$$\left(\frac{\partial V}{\partial Q_2}\right)_{Q_{3,..}} = \frac{1}{\sqrt{2}}\left[\left(\frac{\partial V}{\partial Q_A}\right)_{Q_{B,..}} - \left(\frac{\partial V}{\partial Q_B}\right)_{Q_{A,..}}\right] \tag{40}$$

Substituting eq 40 and 39 into eq 37 gives

$$l_2^{(1,2)} = \frac{-1}{\sqrt{2}}\left\langle b_2(A)\middle|\left(\frac{\partial V}{\partial Q_A}\right)_{Q_B}\middle|b_2(A)\right\rangle = \frac{-1}{\sqrt{2}}l^{PKS} \tag{41}$$

where l^{PKS} is the l of the PKS model.[4] It thus follows that

$$\lambda_2^{(1,2)} = (-1/\sqrt{2})\lambda^{PKS} \tag{42}$$

Introducing eq 42 and our $\lambda_3^{(2)} = 0$ result obtained above into eq 23, we obtain

$$\begin{bmatrix} 0 & -h\upsilon_2\lambda^{PKS}q_2 \\ -h\upsilon_2\lambda^{PKS}q_2 & \Delta + \sqrt{2}h\upsilon_1\lambda_1^{(2)}q_1 \end{bmatrix} \tag{43}$$

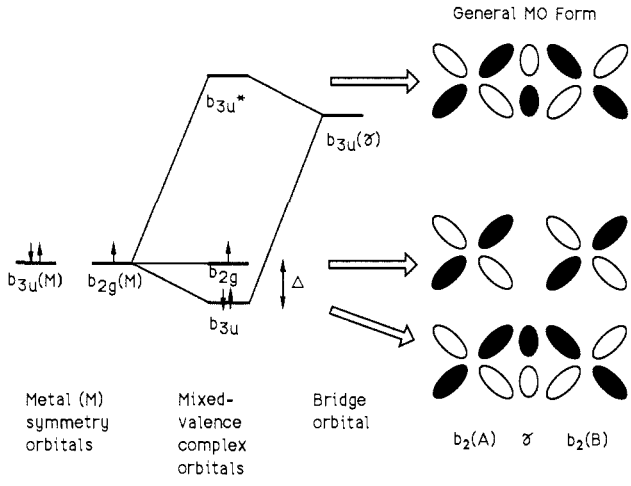

Figure 1. Schematic MO diagram for a mixed-valence complex in which an unoccupied b_{3u} bridge orbital interacts with a b_{3u} metal symmetry orbital.

Aside from the important new term in $\lambda_1^{(2)}$, this is essentially identical with the potential energy matrix of the PKS model (see eq 21 of ref 4). Here, however, we express matrix elements in energy units, rather than units of $h\nu$. Thus,

$$\Delta/h\nu_2 = 2\epsilon^{PKS} \tag{44}$$

where $h\nu_2 = h\nu^{PKS}$. There is also a phase difference in the off-diagonal OVC.

We now use eq 43 as the potential energy matrix in the solution of the dynamic problem. Since $\lambda_3^{(2)} = 0$, q_3 is decoupled and our *simplified MO* model reduces to a two-mode problem with the dimension of eq 30. Thus the simpler basis

$$\Phi_s \equiv [\Phi_{jn_1n_2}]_s \equiv [\varphi_j{}^0\chi_1{}^{n_1}\chi_2{}^{n_2}]_s \tag{45}$$

replaces that of eq 24 in all calculations.

VI. Extent of Valence Trapping

The extent of valence trapping (localization) in a mixed-valence complex can be estimated from a plot of $P(q_2)$, the probability distribution in $q_2 = q_- = (1/\sqrt{2})(q_A - q_B)$ space, versus q_2.[5] A completely *localized* complex will be most stable with equilibrium bond lengths either those of A oxidized and B reduced ($q_A < q_B$ or $q_- < 0$) or those of B oxidized and A reduced ($q_B < q_A$ or $q_- > 0$). This leads to two maxima in the $P(q_2)$ versus q_2 plot which are symmetrically disposed about $q_2 = 0$. At the other extreme, a *delocalized* complex will have a single maximum in the $P(q_2)$ versus q_2 plot at $q_2 = 0$ since the stable complex corresponds to one in which $q_A = q_B$.

Calculation of $P(q_2)$ is straightforward. For each populated vibronic level Ψ_r we find $P_r(q_2)$ by integrating $|\Psi_r|^2$ over all electronic coordinates and over all nuclear coordinates other than q_2. Then $P(q_2)$ is found by summing the Boltzmann-weighted $P_r(q_2)$. Thus

$$P(q_2) = \sum_r \frac{N_r P_r(q_2)}{N}$$

$$P_r(q_2) = \sum_{s=1}^{n_s}\sum_{s'=1}^{n_s} c_{rs}c_{rs'}[\delta_{jj'}\delta_{n_1n_1'}\chi_{n_2(q_2)}\chi_{n_2'}(q_2)]_{ss'} \tag{46}$$

Here the notation is that of eq 32 and 45. $\chi_{n_2}(q_2)$ and $\chi_{n_2'}(q_2)$ are harmonic oscillator functions which have the form

$$\chi_n(q) = \left(\frac{1}{2^n n!\sqrt{\pi}}\right) e^{-q^2/2} H_n(q) \tag{47}$$

where the $H_n(q)$ are Hermite polynomials.

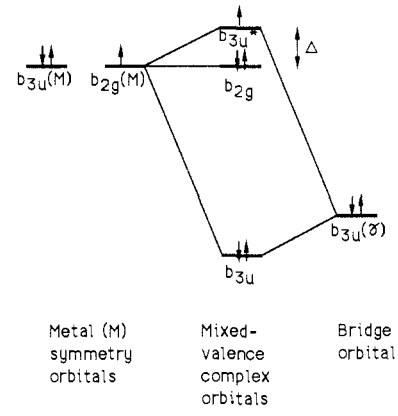

Figure 2. Schematic MO diagram for a mixed-valence complex in which an occupied b_{3u} bridge orbital interacts with a b_{3u} metal symmetry orbital. The MO's have the same general form as in Figure 1.

We calculate $P(q_2)$ and plot it versus q_2 for each set of parameters used to diagonalize our vibronic matrix. The system is considered delocalized when the resulting curve has a single maximum.

VII. Modifications in the *Simplified MO* Model for Typical Mixed-Valence Systems

So far we have not explicitly considered the bridge and how its nature will affect properties of mixed-valence ions. Figures 1 and 2 diagram two common possibilities. In both cases the direct interaction between d orbitals on A and B ($b_2(A)$ and $b_2(B)$ of eq 39) is now assumed negligible so that prior to interaction with bridge orbitals, the b_{2g} and b_{3u} MO's of eq 39 are degenerate symmetry orbitals. We assume the metal d orbitals are the highest occupied orbitals. A bridge MO (or bridging ligand AO) of b_{3u} symmetry forms bonding and antibonding MO's with the b_{3u} metal symmetry orbital, while the b_{2g} metal symmetry orbital is a nonbonding MO. In Figure 1 the interacting bridge MO, $\gamma(b_{3u})$, lies higher in energy and in Figure 2 lower in energy than the metal symmetry orbitals. Δ now becomes the energy difference indicated in the figures. The mixed-valence transition in Figure 1 is $b_{3u} \rightarrow b_{2g}$ (as in the *simplified MO* model) with b_{3u} a bonding MO, while in Figure 2 it is $b_{2g} \rightarrow b_{3u}{}^*$ with $b_{3u}{}^*$ an antibonding MO.

From our discussion of OVC's in section V, we see that in these two cases $l_1^{(1)}$ and $l_3^{(1)}$ will again be zero. For a Figure 1 system $l_\alpha^{(2)}$ ($\alpha = 1, 3$) is defined as in eq 36, while for a Figure 2 complex

$$l_\alpha^{(2)} = -\left\langle b_{2g}\left|\left(\frac{\partial v(i)}{\partial Q_\alpha}\right)_{Q_0}\right|b_{2g}\right\rangle + \left\langle b_{3u}{}^*\left|\left(\frac{\partial v(i)}{\partial Q_\alpha}\right)_{Q_0}\right|b_{3u}{}^*\right\rangle = -[\text{equation 36 with } b_{3u}{}^* \text{ replacing } b_{3u}] \tag{48}$$

In both cases the b_{2g} OVC for q_1 should be negligible since b_{2g} is a nonbonding MO. Then the b_{3u} OVC for q_1 for a Figure 1 complex should be positive since b_{3u} is bonding, but the $b_{3u}{}^*$ OVC for the same coordinate for a Figure 2 complex should be negative since $b_{3u}{}^*$ is antibonding. Thus in both cases $l_1^{(2)}$ (and hence $\lambda_1^{(2)}$) is negative as in the *simplified MO* model. Our definition of $q_1 = q_{AB}$ (Q_{AB} in section III) was general enough to include the appropriate vibration in the Figure 1 and 2 systems.

Since q_A and q_B are localized on the metal ion centers, the bridge-orbital part of the b_{3u} MO's makes no contribution to the b_{3u} OVC for q_3. For this reason $l_3^{(2)}$ will no longer be zero in either Figure 1 or Figure 2 type complexes (as it was in the *simplified MO* model). However, the metal contribution to b_{3u} in Figure 1 and to $b_{3u}{}^*$ in Figure 2 should dominate so there should still be a substantial amount of cancellation. Moreover, in many mixed-valence complexes the d orbitals on A and B relevant to our discussion are t_{2g} orbitals which are nonbonding with respect to the metal ion centers. Thus the diagonal OVC for q_A or q_B involving these orbitals should be negligible. Since the OVC which contribute to $l_3^{(2)}$ may be expressed as linear combinations of these metal-center OVC, it follows that $l_3^{(2)}$ (and hence $\lambda_3^{(2)}$) should once again be negligible as in the *simplified MO* model.

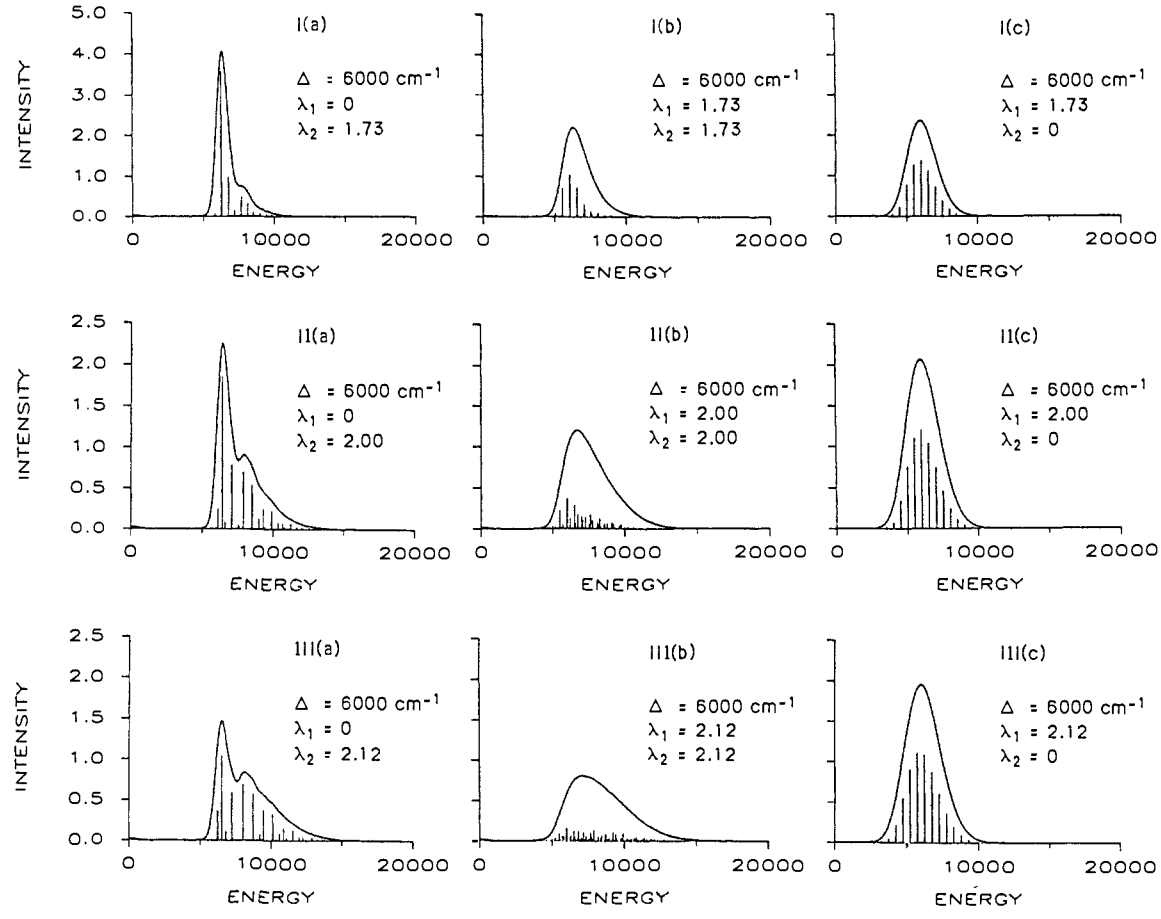

Figure 3. Calculated absorption contours at 298 K. For further details, see section VIII.

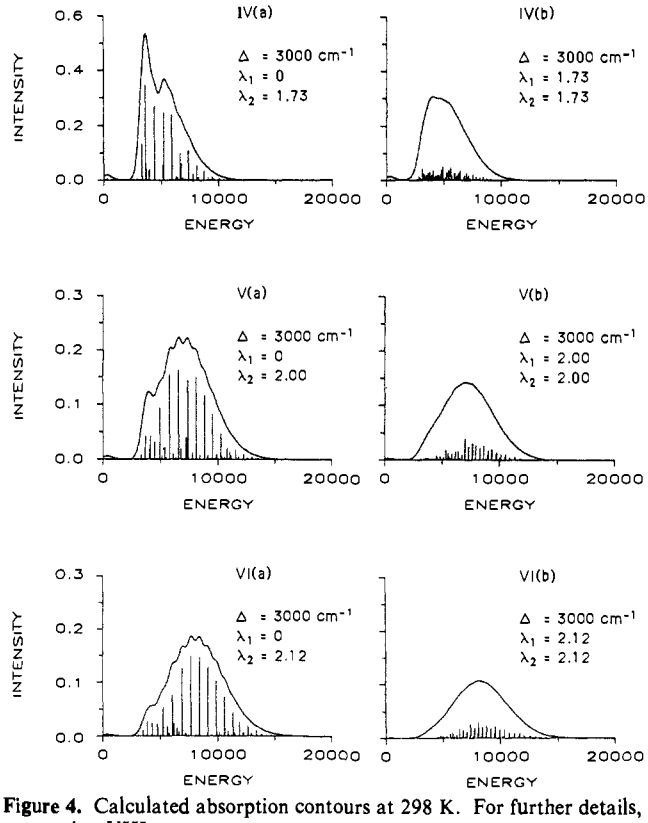

Figure 4. Calculated absorption contours at 298 K. For further details, see section VIII.

Our discussion of $l_2^{(1,2)}$ from section V also applies here. However, the bridge-orbital part of the b_{3u} MO makes no contribution to $l_2^{(1,2)}$ for the same reasons as for $l_3^{(2)}$ above; consequently when the MO interaction is large, $l_2^{(1,2)}$ should be reduced in value.

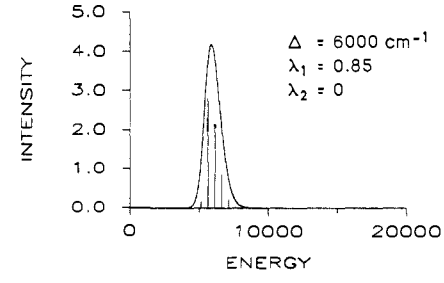

Figure 5. Calculated absorption contour at 298 K. For further details, see section VIII.

Thus we conclude that our *simplified MO* model has the same vibronic interaction matrix (eq 23) as the Figure 1 and Figure 2 systems; the only differences are that Δ *now has a new definition as mentioned above and the magnitude of* $l_2^{(1,2)}$ (*and hence* $\lambda_2^{(1,2)}$) *will be expected to decrease for a given system as* Δ *increases.* Similar results would be obtained if the interaction were between b_{2g} (rather than b_{3u}) bridge and metal-symmetry orbitals.

Of course, the Figure 1 and Figure 2 systems are *still* simplified MO pictures. In a forthcoming paper[13] we will treat a specific system and show how the mixed-valence bandshape and g values are affected by spin–orbit coupling and other perturbations in addition to those interactions included here.

Finally, we note that to make use of the model for real systems, one must have a good idea of which electronic states and which vibrational modes are important to the problem of interest. Here electronic structure calculations, spectroscopic and X-ray diffraction results, and chemical intuition are important sources of information. If the geometry (and hence the point group) were

(13) Piepho, S. B., manuscript in preparation.

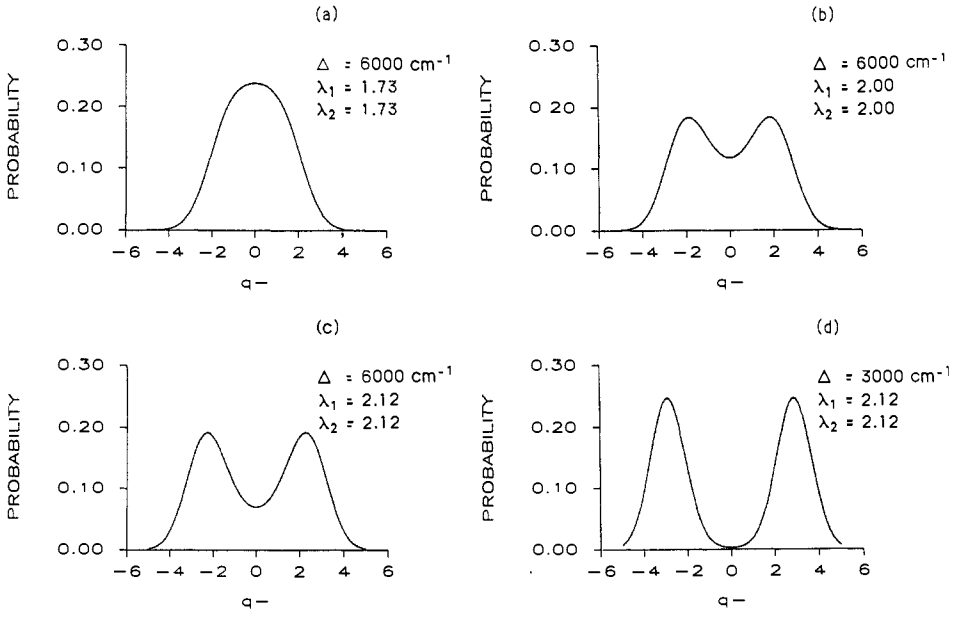

Figure 6. Calculated probability distribution, $P(q_2) = P(q_-)$, versus $q_2 = q_-$ at 298 K. Details of the calculation are described in section VI.

different in an excited state from that in the ground state, all electronic basis states would be defined in the lower point group and vibronic coupling would be expected to be strong in the vibrational coordinate which links the two geometries; thus in our model, λ for that coordinate would be large.

VIII. *Simplified MO* Model Results

Figures 3–5 show the effect of vibronic coupling to q_1, to q_2, or to both q_1 and q_2 simultaneously in the *simplified MO* model for $\Delta = 6000$ cm^{-1} and $\Delta = 3000$ cm^{-1}. Figure 3, I(a)–III(a), and Figure 4, IV(a)–VI(a), give results for vibronic coupling to $q_2 = (1/\sqrt{2})(q_A - q_B)$; this mode is q_- of the PKS model[4] which should be strongly coupled in *localized* mixed-valence compounds. In Figure 3, I(c)–III(c), and in Figure 5 the active mode is $q_1 = q_{AB}$, the multi-center A–B stretching mode; this is the mode that should be strongly coupled in *delocalized* mixed-valence compounds. Then in Figure 3, I(b)–III(b), and Figure 4, IV(b)–VI(b), results are given for the two-mode case.

The total number of vibrational quanta (n in eq 27) used in the calculations was 30. The band shape does not change appreciably when more quanta are used; in fact there is little change in results in going from 20 to 30 total quanta. Thus the vibronic calculation is essentially exact within the context of the model.

Vibrational frequencies were set at 500 cm^{-1} for both q_1 and q_2. The λ values were chosen to best illustrate the features of the model. Values of $\lambda_1^{(2)}$ were chosen so that $\lambda_1^{(2)} = \lambda_2^{(1,2)} = (-1/\sqrt{2})\,\lambda^{PKS}$; results are independent of the sign of λ. In the figures, $\lambda_1 = \lambda_1^{(2)}$ and $\lambda_2 = \lambda_2^{(1,2)}$. The spectra were simulated by using a Gaussian line shape with a line width of 500 cm^{-1}. The stick spectra give the maxima of the Gaussian curves for individual vibronic lines. We plot $D(r \rightarrow r') \times E(r \rightarrow r')$ versus $E(r \rightarrow r')$ where $D(r \rightarrow r')$ is defined in eq 31 and $E(r \rightarrow r') = E_{r'} - E_r$. The simulated intensity is thus directly proportional to the experimental absorbance.

Band Shape and Intensity. The band shape is strongly influenced by the nature of the vibronic coupling. Except at very small $\lambda_1^{(2)}$, coupling to q_1 alone gives rise to a symmetric band of constant intensity centered near Δ which gets broader as $\lambda_1^{(2)}$ increases. Figure 5 illustrates the very narrow asymmetric band predicted at very low $\lambda_1^{(2)}$ while Figure 3, I(c)–III(c), illustrates the more typical symmetric band obtained for larger $\lambda_1^{(2)}$.

In contrast to the above, coupling to $q_2 = q_-$ alone more typically leads to an asymmetric band [Figure 3, I(a)–III(a), and Figure 4, IV(a)] which rises rapidly to a peak near $\Delta + h\nu_2$ with weaker absorption at higher energy. Only when $\lambda^2 \gg \epsilon$ does the band become symmetric [Figure 4, V(a)–VI(a)] with a peak well above Δ. In this limit, the localized extreme, the band intensity is very weak. For a given Δ, the band broadens and its intensity decreases as λ^{PKS} (or $\lambda_2^{(1,2)}$) increases [Figure 3, I(a)–III(a), and Figure 4, IV(a)–VI(a)].

Finally, coupling to both q_1 and q_2 simultaneously [Figure 3, I(b)–III(b), and Figure 4, IV(b)–VI(b)] decreases the band intensity and leads to a smoother and somewhat less asymmetric band shape than for coupling to q_2 alone.

Comparison of analogous parts of Figures 3 and 4 shows that decreasing Δ from 6000 to 3000 cm^{-1} leads to a more symmetric and considerably less intense band.

Low-Energy Infrared Transitions. Low-energy infrared transitions are transitions between low-lying vibronic levels of opposite parity. These transitions gain intensity through vibronic coupling in the PJT-active mode, $q_2 = q_-$. Thus they appear *only* when λ^{PKS} (or, equivalently $\lambda_2^{(1,2)}$) is nonzero. In localized systems they are often called tunneling transitions.

For a given Δ low-energy infrared transitions become weaker as λ^{PKS} increases. The reason for this is that while $|\langle\Psi_r|m_z|\Psi_{r'}\rangle|^2$ becomes larger for a given $\Psi_r \rightarrow \Psi_{r'}$ transition as $\lambda_2^{(1,2)}$ increases, $E(r \rightarrow r')$ and hence $(N_r - N_{r'})/N$ become smaller; the net result is that the intensity, $D(r \rightarrow r') \times E(r \rightarrow r')$, decreases with increasing λ^{PKS}. The intensity of the low-energy infrared transitions in Figure 3 is in all cases ≤0.50% of the total band intensity illustrated. Here we consider all transitions ≤1000 cm^{-1} to be low-energy infrared transitions. For a given set of vibronic coupling parameters, these transitions increase in intensity as Δ increases, but the percent of the total intensity they represent decreases.

Extent of Valence Trapping. Figure 6 illustrates how the extent of valence trapping is related to the model parameters. As Δ and λ^{PKS} increase, the system becomes more and more localized (valence trapped). Comparison of Figure 4, VI(b), with Figure 6d shows that by the time λ^{PKS} has increased sufficiently to give a symmetric mixed-valence band the system is completely localized: $P(q_-) = 0$ at $q_- = 0$. A smaller effect (which we do not illustrate in our figures) is that if $\lambda_1^{(2)}$ is increased while all other parameters are held constant the system becomes slightly more localized.

Effect of Temperature. The effect of temperature on the mixed-valence band shape and on the extent of valence trapping is illustrated in Figure 7. In particular note that the system is more delocalized at low temperature.

IX. Discussion

Our results demonstrate how the mixed-valence band shape is influenced by electronic and vibronic coupling. In the delocalized limit when coupling is primarily to $q_1 = q_{AB}$, a relatively intense

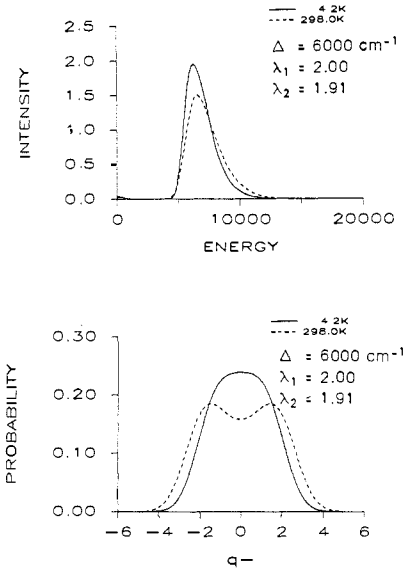

Figure 7. Calculated absorption contour and $P(q_2) = P(q_-)$ probability distribution at 4.2 and 298 K for the indicated parameters.

symmetric band centered at approximately Δ is typical [Figure 3, I(c)–III(c)]. The exception to this is the very narrow asymmetric band which occurs when the coupling to q_1 is extremely weak (Figure 5). When there is *no* coupling to q_2, *no* low-energy infrared transitions are predicted. However, it is arguable whether in this limit we still have a "mixed-valence" system since the two oxidation states have completely lost their identity.

Coupling to q_2 leads to an asymmetric band shape except when the coupling is very strong. A symmetric band shape is predicted in the localized (valence trapped) limit in which $(\lambda^{PKS})^2 \gg \epsilon$; then a broad, weak band is obtained [Figure 4, VI(a)–VI(b)] which peaks near $(\lambda^{PKS})^2 \times 2h\nu_2$ as predicted by Hush.[3] The major effect of coupling to $q_1 = q_{AB}$ in addition to q_2 is a general smoothing of the band shape and a reduction in band intensity.

While the results given above are for our *simplified MO* model system, we show in section VII that with redefinition of Δ, they also apply for the more realistic (but still over-simplified) Figure 1 and Figure 2 systems. Moreover, they suggest the dominant features that will govern the line shape in real compounds. The major differences between the simple systems described above and a real mixed-valence compound are that the latter can have more than one band with mixed-valence character and the q_3 mode no longer completely decouples. Real systems will have a number of nonbonding orbitals that may be involved in low-energy excitations. All the resulting low-lying states become mixed by spin–orbit coupling. Nonetheless, the band shape of the mixed-valence transitions in these more complex compounds should follow the general pattern outlined above for the *simplified MO* model. The one obvious additional complication is that band asymmetry may result from two overlapping transitions. The effect of vibronic coupling to q_3 is similar to that for q_1.

It is of interest to compare the present *simplified MO* model to the work of Ondrechen et al.[11] and to the PKS model.[4,5] Ondrechen et al. employ a three-site MO model for delocalized (class III) bridged mixed-valence dimers which have the form A–B–C where A and C are metal ion centers and B is a bridging ligand. They stress the importance of coupling to totally symmetric modes in bridged systems. Their electronic basis is essentially that of Figure 1 with the three-site equivalent of q_1 weakly coupled and coupling to q_2 negligible; coupling to q_3 is also included. The nature of their results[11c,d,g] is very similar to our case pictured in Figure 5. For the reasons we outline in section VII, our *simplified MO* model spectra, such as those of Figures 3–5, may be used to understand the Figure 1 and Figure 2 systems. Since Ondrechen et al.'s parameters are analogous to those used in Figure 5, similar results are obtained. One difference is that Ondrechen et al. include weak coupling to q_3 which we argue is negligible. However, this weak coupling has little additional effect on the band shape.

While Ondrechen et al.'s results are limited to delocalized systems, ours (like the PKS model) are applicable to the *full range* of mixed-valence systems from completely valence delocalized to valence trapped. Since our results may be determined to arbitrary accuracy by using a sufficiently large vibrational basis, they may be made essentially "exact" within the context of the model.

Ondrechen et al. also apply an extended version of their model to the Creutz–Taube ion.[11e,f,g] We leave discussion of such systems to a later paper.[13]

Our *simplified MO* model differs from the PKS model in a number of significant respects. The most important difference is the inclusion of vibronic coupling to the multi-center mode, $q_1 = q_{AB}$. The PKS model considered only single center modes localized on A and on B. We demonstrate above that coupling to q_1 has a significant effect on the band shape. In the delocalized limit when coupling to q_1 dominates, low-energy infrared transitions are negligible; however, in that case the two oxidation states have completely lost their identity and we no longer really have a "mixed-valence" system. A second difference between our model and the PKS approach is that the PKS model uses a valence-bond type basis while we follow Ondrechen et al. and use a MO type basis. The main reason for the switch to the MO basis is that it proves much simpler to extend our *simplified MO* model to more complex mixed-valence systems with the MO basis.

We also introduce Bersuker's[12] orbital vibronic constants (OVC). The magnitude of the OVC govern the magnitude of vibronic coupling. Since they are orbital constants, they should have similar values in related systems. Moreover, the magnitude of OVC may be estimated by consideration of the type of MO's and vibrations involved. As we illustrate in earlier sections, this proves extremely valuable in determining which molecular vibrations are likely to be strongly coupled vibronically.

Acknowledgment. This work was supported under National Science Foundation Grants CHE8604470 and RII-8600354, and in part under CHE8400423. Some of the calculations were made possible by a grant of time by the Pittsburgh Supercomputing Center. I also acknowledge many useful discussions with Professor Paul N. Schatz, and the able assistance of Kelly Lenz and Suzanne Szak with the computer programming. Thanks also go to the University of Virginia for its hospitality during my year there under the NSF/VPW program.